vibration

MDPI

Article

A Nonlinear Approach to the Delamination Characterization of Solid Structures Using Impact Response—Part II: Volterra-Series Formulation and Bispectral Analysis

Yousef Sardahi [1,*], Asad Salem [2], Loulin Huang [3], Isaac Wait [4] and Gang S. Chen [1,*]

[1] Department of Mechanical and Industrial Engineering, College of Engineering and Computer Science, Marshall University, Huntington, WV 25755, USA
[2] Battery Research Institute, Marshall University, Huntington, WV 25755, USA; asad.salem@marshall.edu
[3] School of Engineering, Computer and Mathematical Sciences, Auckland University of Technology (AUT), Auckland 1010, New Zealand; loulin.huang@aut.ac.nz
[4] Department of Civil Engineering, College of Engineering and Computer Science, Marshall University, Huntington, WV 25755, USA; isaac.wait@marshall.edu
* Correspondence: sardahi@marshall.edu (Y.S.); chenga@marshall.edu (G.S.C.)

Abstract

This study develops a third-order Volterra-series and bispectral framework for examining nonlinear vibration behavior at a delaminated region under impact excitation. The local response is represented by a nonlinear oscillator with quadratic and cubic stiffness terms, and the corresponding Volterra formulation relates these terms to the fundamental, second-harmonic, and third-harmonic response components. Bispectral analysis is then applied to measured responses above an artificial delamination under very small and small impact conditions. Within the calibrated frequency region, the very-small-impact response exhibits a relatively concentrated bispectral distribution, whereas the small-impact response exhibits a broader and more distributed pattern. The third-order cumulant shows a corresponding change from a localized to a more distributed lag-domain structure. Because the records are independently normalized, absolute bispectrum magnitudes are not compared quantitatively. An equal-duration sensitivity analysis using 614 samples for both conditions confirmed that the broader small-impact bispectral distribution persists after controlling for record duration. The results demonstrate how bispectral measures complement conventional spectral analysis by describing changes in third-order statistical structure and phase relationships among frequency components. The findings are interpreted as a proof-of-concept comparison at a known delamination location rather than as a generalized delamination-identification criterion.

Keywords: nonlinear vibration; delamination detection; impact response; impact echo; Volterra series; bispectrum; higher-order spectrum; structural health monitoring; concrete structures

Check for updates

Academic Editors: Mohamed Ichchou and Noureddine Bouhaddi

Received: 18 August 2026
Revised: 1 September 2026
Accepted: 4 September 2026
Published: 9 September 2026

1. Introduction

Impact-response techniques are widely employed in the nondestructive assessment of solid structures since they are able to detect subsurface defects such as cracks, voids, and delamination; these defects alter the local stiffness and dynamic response of the structure. Impact-echo methods have therefore been used to evaluate delamination and internal defects in concrete structures [1]. Recent studies have also shown that defects can introduce nonlinear features into impact-echo responses [2]. For a delaminated region, the separated interfaces can open, close, or interact during vibration [3]. This behavior can generate harmonics and other frequency components that are absent from a purely linear response.

Recent nondestructive-testing developments also include noncontact laser-ultrasonic methods for localized defect and material characterization in additively manufactured structures, as well as data-driven methods for detecting changes in measured structural vibration responses [4–6]. These studies illustrate the broader trend toward extracting local or response-sensitive features beyond conventional global spectral indicators.

Nonlinear vibration methods have received increasing attention in structural health monitoring. They can provide damage-sensitive features when changes in linear modal properties are small. Hammami et al. [7] studied composite structures with controlled delamination and reported changes in their nonlinear vibration behavior. Dolbachian et al. [8] reviewed linear and nonlinear vibration methods for structural health monitoring and discussed the value of nonlinear response features for damage detection. Related studies have shown that crack opening and closing can produce higher harmonics and other nonlinear vibration characteristics [9]. These results support the use of nonlinear vibration measurements for detecting contact-type defects. Recent nonlinear-vibration studies in other structural applications have also demonstrated how nonlinear stiffness, adjustable structural parameters, and amplitude-dependent dynamics can substantially alter measured vibration responses [10,11].

Conventional frequency-domain methods remain useful for identifying dominant frequencies and harmonics. The fast Fourier transform (FFT) and power spectral density are commonly used for this purpose. However, these measures do not directly describe phase coupling between different frequency components. This information becomes important when nonlinear interactions are present. For example, two frequency components may interact and produce another component while maintaining a fixed phase relationship. A conventional power spectrum cannot determine whether these components are independent or are related through nonlinear coupling [12,13].

Higher-order spectral analysis provides additional information about such interactions. Unlike second-order spectra, higher-order spectra retain information about statistical dependence among multiple frequency components [12,13]. The bispectrum is the lowest-order spectrum beyond the power spectrum. It is the two-dimensional Fourier transform of the third-order cumulant. It can reveal quadratic phase coupling among frequency components. It is also less sensitive to independent additive Gaussian noise because the theoretical third-order cumulant of a Gaussian process is zero [12,13].

Bispectral methods have been applied to several nonlinear vibration problems. Rivola and White [14] used bispectral analysis to study a bilinear oscillator and fatigue-crack behavior. Hillis et al. [15] applied the method to global crack detection. Nichols et al. [16] investigated auto-bispectral density for detecting quadratic nonlinearities in structural systems. Nichols and Olson [17] later studied the detection of weak quadratic nonlinearities. Higher-order spectra have also been used to identify nonlinear modal coupling [18].

Bispectral analysis has also been applied directly to structural damage problems. Cui et al. [19] studied beam-type structures containing a breathing crack and showed that bispectral features are sensitive to the associated nonlinear response. More recent studies have applied higher-order spectral methods to nonlinear vibro-acoustic modulation for structural damage detection [20], micro-crack localization in steel strands [21], and microcrack detection using an S-transform bispectrum [22]. Together, these studies show that higher-order spectra can reveal damage-related frequency interactions that may not be clear from conventional spectra alone.

A mathematical description of nonlinear input–output behavior can be obtained from the Volterra series. The Volterra series extends linear convolution by introducing higher-

https://doi.org/10.3390/vibration9030057

order kernels [23]. The first-order kernel describes the linear response. Higher-order kernels describe nonlinear contributions. Their multidimensional Fourier transforms define higher-order frequency-response functions. These functions describe how nonlinear terms contribute to harmonics and frequency interactions.

Volterra-series models have been widely studied for nonlinear system identification [24,25]. Their ability to separate linear and nonlinear response contributions has also led to their use in structural damage detection. Shiki et al. [26] used a discrete-time Volterra model for damage detection in an initially nonlinear system. Villani et al. [27] used stochastic Volterra-series models to detect damage in nonlinear structures while accounting for uncertainty. These studies show that Volterra kernels can be used to relate measured structural responses to different orders of nonlinear behavior.

Part I of the present study developed a nonlinear approach for characterizing delamination from impact-response measurements [3]. The delaminated region was represented by a nonlinear oscillator. Perturbation and harmonic-balance methods were used to describe its response. The results showed that higher-order harmonics can provide information about the nonlinear behavior of the delaminated region. The experimental signals were examined mainly using the FFT and power spectrum. These methods clearly identify dominant frequencies and generated harmonics. However, they do not directly quantify phase coupling among the frequency components. The perturbation-based formulation is also most suitable when the nonlinear terms remain sufficiently small.

The present study extends Part I in two directions. First, the nonlinear impact response is represented using a Volterra series. The response is expressed in terms of higher-order kernels and higher-order frequency-response functions. A third-order representation is used to relate the quadratic and cubic stiffness terms to the fundamental, second-harmonic, and third-harmonic response components. Second, bispectral analysis is applied to the experimental impact-response signals reported in Part I. Responses measured at the delamination location under very small and small impact excitations are compared using the third-order cumulant, bispectrum magnitude, and bispectrum phase. The objective is to determine whether changes in higher-order spectral structure provide information about the nonlinear response that is not available from the conventional power spectrum alone. The present Part II analysis is intended primarily to characterize changes in higher-order spectral structure at a known delamination location. It does not independently establish spatial localization or quantitative delamination severity. Localization would require measurements over multiple spatial positions, while severity estimation would require calibration against defects with systematically varied geometry and interface conditions.

The remainder of this paper is organized as follows. Section 2 describes the Volterra-series model of the system and the higher-order spectral measures used throughout the paper. Section 3 describes the application of the higher-order spectral analysis to the experimental impact response data and the comparison of the two excitation conditions. Closing remarks, study limitations, and recommendations for future work are provided in Section 4.

2. Volterra-Series Formulation and Higher-Order Spectral Characterization

2.1. Nonlinear Dynamic Model

Part I represented the local response of a delaminated solid structure using a nonlinear oscillator model [3]. Following that formulation, the response is written as

$$m\ddot{x}(t) + c\dot{x}(t) + k_1 x(t) + k_2 x^2(t) + k_3 x^3(t) + \cdots = F(t), \tag{1}$$

https://doi.org/10.3390/vibration9030057

where $x(t)$ is the local structural response, $F(t)$ is the applied excitation, m is the equivalent mass, c is the damping coefficient, k_1 is the linear stiffness, and k_2 and k_3 are the quadratic and cubic stiffness coefficients, respectively.

The perturbation formulation used in Part I assumes that the nonlinear contribution remains sufficiently small. Here, the response is represented using a Volterra series. This representation breaks the response into contributions of successive input orders [23–25]:

$$x(t) = x_1(t) + x_2(t) + x_3(t) + \cdots . \quad (2)$$

The nth-order contribution is

$$x_n(t) = \int_{-\infty}^{\infty} \cdots \int_{-\infty}^{\infty} h_n(\tau_1, \ldots, \tau_n) \prod_{r=1}^{n} F(t - \tau_r)\, d\tau_1 \cdots d\tau_n, \quad (3)$$

where $h_n(\tau_1, \ldots, \tau_n)$ is the nth-order Volterra kernel. The first-order kernel gives the linear response. Higher-order kernels describe nonlinear contributions.

For the underdamped linearized system, where $0 \leq \zeta < 1$, we define

$$\omega_n = \sqrt{\frac{k_1}{m}}, \qquad \zeta = \frac{c}{2m\omega_n}, \qquad \omega_d = \omega_n\sqrt{1 - \zeta^2}. \quad (4)$$

The first-order impulse-response function is

$$h_1(t) = \frac{1}{m\omega_d} e^{-\zeta\omega_n t} \sin(\omega_d t) u(t), \quad (5)$$

where $u(t)$ is the unit-step function.

The multidimensional Fourier transform of the nth-order Volterra kernel defines the corresponding higher-order frequency-response function (HFRF) [24,25]:

$$H_n(\Omega_1, \ldots, \Omega_n) = \int_{-\infty}^{\infty} \cdots \int_{-\infty}^{\infty} h_n(\tau_1, \ldots, \tau_n) e^{-j\sum_{r=1}^{n} \Omega_r \tau_r}\, d\tau_1 \cdots d\tau_n. \quad (6)$$

For $n = 1$, Equation (6) gives the dimensional linear frequency-response function

$$H_1(\Omega) = \frac{1}{k_1 - m\Omega^2 + jc\Omega}. \quad (7)$$

This dimensional form is used throughout the following derivation. It avoids the need to introduce normalized nonlinear stiffness coefficients.

2.2. Higher-Order Frequency-Response Functions

The Volterra series is retained through third order. Substitution of Equation (2) into Equation (1), followed by collection of terms of equal input order, yields the second- and third-order HFRFs [24,25].

The second-order HFRF is

$$H_2(\Omega_1, \Omega_2) = -k_2 H_1(\Omega_1 + \Omega_2) H_1(\Omega_1) H_1(\Omega_2). \quad (8)$$

Assuming symmetric Volterra kernels, the third-order HFRF is given by

$$\begin{aligned} H_3(\Omega_1,\Omega_2,\Omega_3) = & -H_1(\Omega_1+\Omega_2+\Omega_3)\Bigg[k_3\prod_{r=1}^{3}H_1(\Omega_r) \\ & + \frac{2k_2}{3}\Big(H_1(\Omega_1)H_2(\Omega_2,\Omega_3) \\ & \qquad + H_1(\Omega_2)H_2(\Omega_1,\Omega_3) \\ & \qquad + H_1(\Omega_3)H_2(\Omega_1,\Omega_2)\Big)\Bigg]. \end{aligned} \tag{9}$$

Equations (8) and (9) show that the higher-order response depends on the nonlinear stiffness coefficients k_2 and k_3.

Consider a harmonic excitation

$$F(t) = A\cos(\omega t), \tag{10}$$

where A is the excitation amplitude and ω is the angular excitation frequency. For compact notation, we define

$$H_n^{p,q}(\omega) = H_n(\underbrace{\omega,\ldots,\omega}_{p},\underbrace{-\omega,\ldots,-\omega}_{q}), \qquad p+q=n. \tag{11}$$

The required second-order terms are

$$H_2^{2,0}(\omega) = -k_2 H_1(2\omega)H_1^2(\omega), \tag{12}$$

and

$$H_2^{1,1}(\omega) = -k_2 H_1(0)H_1(\omega)H_1(-\omega). \tag{13}$$

For a system with real coefficients,

$$H_1(-\omega) = H_1^*(\omega), \tag{14}$$

where $(\cdot)^*$ denotes complex conjugation.

Using Equation (9), the third-order HFRF associated with the fundamental frequency is

$$\begin{aligned} H_3^{2,1}(\omega) = & \, H_1^3(\omega)H_1(-\omega) \\ & \times\left\{\frac{2k_2^2}{3}[H_1(2\omega)+2H_1(0)] - k_3\right\}. \end{aligned} \tag{15}$$

The third-order HFRF associated with the third harmonic is

$$H_3^{3,0}(\omega) = H_1(3\omega)H_1^3(\omega)\Big[2k_2^2 H_1(2\omega) - k_3\Big]. \tag{16}$$

These expressions relate the nonlinear stiffness coefficients to the harmonic components of the response.

2.3. Harmonic Response

Retaining terms through third order, one can write the steady-state response of Equation (10) as

$$\begin{aligned} x(t) \approx & \, X_0 + |X_1(\omega)|\cos(\omega t+\phi_1) \\ & + |X_2(\omega)|\cos(2\omega t+\phi_2) \\ & + |X_3(\omega)|\cos(3\omega t+\phi_3), \end{aligned} \tag{17}$$

https://doi.org/10.3390/vibration9030057

where

$$\phi_r = \arg[X_r(\omega)]. \tag{18}$$

The leading harmonic coefficients are

$$X_0 = \frac{A^2}{2} H_2^{1,1}(\omega), \tag{19}$$

$$X_1(\omega) = AH_1(\omega) + \frac{3A^3}{4} H_3^{2,1}(\omega), \tag{20}$$

$$X_2(\omega) = \frac{A^2}{2} H_2^{2,0}(\omega), \tag{21}$$

and

$$X_3(\omega) = \frac{A^3}{4} H_3^{3,0}(\omega). \tag{22}$$

Substitution of Equations (12) and (15) yields

$$\begin{aligned} X_1(\omega) = AH_1(\omega) + \frac{3A^3}{4} H_1^3(\omega) H_1(-\omega) \\ \times \left\{ \frac{2k_2^2}{3} [H_1(2\omega) + 2H_1(0)] - k_3 \right\}, \end{aligned} \tag{23}$$

and

$$X_2(\omega) = -\frac{A^2}{2} k_2 H_1^2(\omega) H_1(2\omega). \tag{24}$$

Equations (20)–(22) show how the nonlinear stiffness generates additional harmonic components. The quadratic term contributes to the zero-frequency and second-harmonic components. The cubic term contributes directly to the fundamental and third-harmonic components. Repeated quadratic interactions also contribute to the third-order response.

Although the experimental excitation is impulsive, the harmonic formulation shows how the quadratic and cubic nonlinearities generate frequency interactions. A broadband impact excites a range of frequency components simultaneously, allowing these nonlinear interactions to appear in the measured response.

Within the third-order model, if $k_2 = k_3 = 0$, then these higher-order kernels vanish. The response then reduces to the linear component. Within the present structural model, the higher-order harmonics therefore provide information about nonlinear contributions to the response. Their experimental interpretation assumes that nonlinear distortion from the excitation and measurement system is negligible.

The third-order truncation is adopted because the present structural model retains quadratic and cubic stiffness terms and the analysis focuses on their leading contributions through the third harmonic. It should therefore be regarded as a model-order assumption rather than as an experimentally demonstrated convergence order. The present study does not identify a complete set of Volterra kernels from measured input–output data, so a residual-based convergence test of successively identified Volterra orders is not available. Higher Volterra orders should be retained when fourth- and higher-order contributions become non-negligible or when the third-order model no longer provides an adequate description of the measured response [23–25].

2.4. Power Spectrum and Bispectrum

The Volterra formulation describes how nonlinear terms generate and couple frequency components. Higher-order spectral analysis provides another way to study these interactions from measured vibration signals [12,13,28].

Let the centered response be

$$\tilde{x}(t) = x(t) - \mu_x, \tag{25}$$

where

$$\mu_x = E[x(t)]. \tag{26}$$

For a stationary process, the second-order autocovariance is

$$R_{xx}(\tau) = E[\tilde{x}(t)\tilde{x}(t+\tau)]. \tag{27}$$

The power spectral density is the one-dimensional Fourier transform of $R_{xx}(\tau)$:

$$P_x(\Omega) = \int_{-\infty}^{\infty} R_{xx}(\tau) e^{-j\Omega\tau}\, d\tau. \tag{28}$$

The third-order cumulant is

$$C_{3,x}(\tau_1, \tau_2) = E[\tilde{x}(t)\tilde{x}(t+\tau_1)\tilde{x}(t+\tau_2)]. \tag{29}$$

The bispectrum is the two-dimensional Fourier transform of the third-order cumulant [12,13]:

$$\begin{aligned} B_x(\Omega_1, \Omega_2) = \int_{-\infty}^{\infty}\int_{-\infty}^{\infty} & C_{3,x}(\tau_1, \tau_2) \\ & \times e^{-j(\Omega_1\tau_1 + \Omega_2\tau_2)}\, d\tau_1\, d\tau_2. \end{aligned} \tag{30}$$

Unlike the power spectrum, the bispectrum contains information about third-order statistical dependence and phase relationships among frequency components [12,13,28]. A nonzero component at (Ω_1, Ω_2) can also indicate the relationship to Ω_1, Ω_2, and the sum frequency $\Omega_1 + \Omega_2$.

For an ideal Gaussian random process, cumulants above second order are zero. Therefore, independent additive Gaussian noise has zero theoretical third-order cumulant and does not contribute to the theoretical bispectrum [12,13]. A finite-record estimate, however, is not expected to be exactly zero.

A nonzero bispectrum is not, by itself, proof of structural nonlinearity. A linear system driven by a non-Gaussian input can also produce a nonzero bispectrum. Accordingly, attribution of a measured bispectral component specifically to structural nonlinearity requires consideration of both the excitation characteristics and an appropriate reference structural response. The bispectral results presented here are therefore interpreted comparatively and not as unique evidence of structural nonlinearity. Finite-record estimation can introduce additional variability [12,28]. For this reason, the present study uses the bispectrum to compare changes in higher-order spectral structure between the two impact conditions.

The impact responses considered in Section 3 are transient and have finite duration. The quantities in Equations (28) and (30) are therefore represented experimentally by finite-record spectral estimates rather than exact ensemble quantities [29]. The bispectrum magnitude and phase distributions are compared between the two impact conditions.

In the experimental analysis presented in the next section, cyclic frequency f is used in place of angular frequency Ω, with $\Omega = 2\pi f$.

https://doi.org/10.3390/vibration9030057

3. Experimental Bispectral Analysis and Discussion

The experimental impact-response signals reported in Part I [3] are examined here using third-order statistical and bispectral analysis. Two excitation conditions are considered: a very small impact and a small impact. The purpose is to compare the higher-order spectral structure of the measured responses and relate the observed changes to the nonlinear behavior discussed in Section 2.

3.1. Experimental Setup and Signal Processing

The experimental signals analyzed in this study were obtained from the concrete specimen and measurement system reported in Part I [3]. The slab dimensions were 812.8 mm × 406.4 mm × 152.4 mm. The artificial delamination was formed using an expanded-polystyrene insert with dimensions 304.8 mm × 304.8 mm × 3.175 mm, with its upper surface located 25.4 mm below the top surface of the slab. The specimen consisted of normal concrete with a reported compressive strength of 27 MPa. The accelerometer was positioned near the center of the region directly above the artificial delamination, and the impact was applied close to the sensor. A simplified representation of the specimen, defect, impact position, and measurement position is shown in Figure 1. Additional photographs and details of the test setup are provided in Part I [3].

Here, "impact response" denotes the transient structural response following a finite-duration mechanical impact. This terminology is distinguished from the ideal impulse-response function used in the theoretical Volterra formulation. The experimental impacts followed the low-to-moderate, nondestructive excitation regime used in Part I [3].

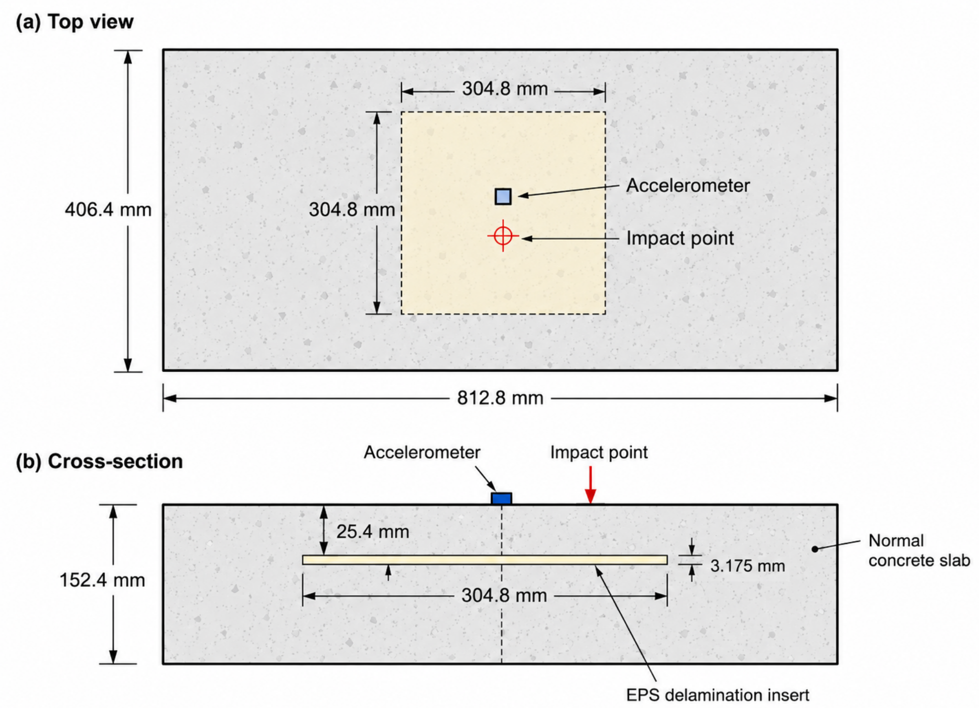

Figure 1. Schematic of the experimental specimen and measurement configuration: (**a**) top view showing the concrete slab dimensions, artificial delamination region, accelerometer location, and nearby impact point; (**b**) cross-sectional view showing the slab thickness, delamination dimensions and depth, accelerometer location, and impact point. The artificial delamination was formed using an expanded-polystyrene insert.

Because the impact and measurement positions are located directly above the artificial delamination, the recorded response is sensitive to the localized flexural dynamics of the

https://doi.org/10.3390/vibration9030057

separated near-surface region. The delamination dimensions, depth, and interface conditions affect the effective local mass, stiffness, boundary conditions, and modal frequencies. The present single-location analysis does not, however, reconstruct an unknown defect position or shape. Spatial localization would require measurements over multiple positions, while quantitative shape or severity estimation would require calibration or an appropriate inverse model.

Acceleration was measured using a PCB Piezotronics Model 352B30 ICP® piezoelectric accelerometer (PCB Piezotronics, Inc., Depew, NY, USA). The sensor has a nominal sensitivity of 10 mV/g, a measurement range of $\pm$500 g_{pk}, and a specified frequency range of 15–4500 Hz within $\pm$5%. It also includes an internal low-pass filter with a corner frequency of 10 kHz and a roll-off of 12 dB/octave [30]. The accelerometer was powered and conditioned using a PCB Piezotronics Model 482A22 four-channel ICP® signal conditioner [31]. The results reported here are based on this measurement chain.

The vibration signals were recorded as uncompressed `.wav` files using Audacity and imported into MATLAB R2026a. The sampling frequency was read from the file header. Both records were sampled at $F_s = 44.1$ kHz. The very-small-impact record contained 614 samples and had a duration of 13.923 ms. The small-impact record contained 1102 samples and had a duration of 24.989 ms. The complete recorded response was retained for each condition. Because the records have different durations, the comparison is made primarily in terms of the distribution and structure of the higher-order spectral components rather than their absolute bispectral magnitudes.

To examine the influence of unequal record duration on the higher-order spectral estimates, an additional equal-duration sensitivity analysis was performed. The complete 614-sample very-small-impact record was used as the reference, and a 614-sample segment was extracted from the small-impact record, giving a common analysis duration of 13.923 ms. The two windows were aligned using the maximum absolute value of the mean-removed response as a reproducible marker of the main impact-response event. The same preprocessing, normalization, maximum lag, Hamming lag window, biased estimator, frequency-triad restriction, and biphase-display criterion were then applied to both records.

Before the higher-order spectral analysis, each record was converted to a single-column signal. If more than one recorded channel was present, the channels were averaged. The sample mean was then removed,

$$x_c(t) = x(t) - \overline{x}, \tag{31}$$

where $\overline{x}$ is the sample mean. Each record was then normalized by its own maximum absolute amplitude,

$$x_n(t) = \frac{x_c(t)}{\max|x_c(t)|}. \tag{32}$$

This normalization removes differences in overall signal scale. It allows the two responses to be compared mainly through their waveform and higher-order spectral structure. Since the signals are normalized independently, absolute bispectrum magnitudes are not used as a quantitative measure of the difference between the two excitation conditions.

The third-order cumulant and bispectrum were estimated using the `bisp3cum` MATLAB routine developed by McMurray [32]. The same processing parameters were used for both records. A maximum lag of 60 samples was used. At $F_s = 44.1$ kHz, this corresponds to

$$\tau_{\max} = \frac{60}{44{,}100} \approx 1.36 \text{ ms}. \tag{33}$$

https://doi.org/10.3390/vibration9030057

A Hamming lag window and a biased cumulant estimator were used. The bispectrum magnitude and phase were calculated as

$$|B_x(f_1, f_2)| \tag{34}$$

and

$$\phi_B(f_1, f_2) = \arg[B_x(f_1, f_2)], \tag{35}$$

respectively, with the phase expressed in degrees. The same preprocessing, maximum lag, lag window, and estimator settings were applied to both impact records.

Although the bispectrum was calculated over the discrete frequency range defined by the sampling frequency, the displayed bispectral results were restricted to avoid interpreting frequency combinations above the specified upper measurement limit of the accelerometer. Since a bispectral component $B_x(f_1, f_2)$ involves the frequency triad f_1, f_2, and $f_1 + f_2$, only combinations satisfying

$$|f_1| \leq 4.5\ \text{kHz}, \qquad |f_2| \leq 4.5\ \text{kHz}, \qquad |f_1 + f_2| \leq 4.5\ \text{kHz} \tag{36}$$

were retained for display and physical interpretation.

For the phase plots, an additional relative-magnitude criterion was applied. The biphase was displayed only where

$$|B_x(f_1, f_2)| \geq 0.05 B_{\max}, \tag{37}$$

where $B_{\max}$ is the maximum bispectrum magnitude within the retained frequency-triad region for the corresponding record. The threshold was therefore calculated separately for each impact condition. It was used only for visualization and does not modify the bispectrum estimate or the magnitude distributions. In the magnitude plots, blank regions denote frequency combinations excluded by Equation (36). In the phase plots, blank regions additionally include locations where the corresponding bispectrum magnitude is below the threshold in Equation (37).

Table 1 summarizes the experimental configuration and processing parameters.

Table 1. Experimental configuration and signal-processing parameters used for the higher-order spectral analysis.

Parameter	Specification or Procedure
Specimen	Concrete slab containing an artificial delamination formed using an expanded-polystyrene insert; complete specimen geometry is reported in Part I [3].
Measurement location	Accelerometer positioned near the center of the region directly above the artificial delamination; impact applied close to the sensor.
Accelerometer	PCB Piezotronics Model 352B30 ICP®; nominal sensitivity 10 mV/g; range ± 500 g_{pk}; specified frequency range 15–4500 Hz ($\pm 5\%$) [30].
Signal conditioner	PCB Piezotronics Model 482A22 four-channel ICP® signal conditioner [31].
Recording format	Uncompressed `.wav` files recorded using Audacity and analyzed in MATLAB R2026a.
Sampling frequency	$F_s = 44.1$ kHz for both records.
Very-small-impact record	614 samples; duration 13.923 ms.
Small-impact record	1102 samples; duration 24.989 ms.

https://doi.org/10.3390/vibration9030057

Table 1. *Cont.*

Parameter	Specification or Procedure
Mean removal	Sample mean removed before normalization and higher-order spectral analysis.
Normalization	Each record independently normalized by its maximum absolute amplitude, as defined in Equation (32).
Maximum lag	60 samples, corresponding to approximately 1.36 ms at $F_s = 44.1$ kHz.
Lag window	Hamming window.
Cumulant estimator	Biased estimate.
Bispectrum magnitude	$\lvert B_x(f_1, f_2) \rvert$.
Bispectrum phase	$\arg[B_x(f_1, f_2)]$, reported in degrees.
Phase display criterion	Biphase displayed only where $\lvert B_x(f_1, f_2)\rvert \geq 0.05 B_{\max}$ within the retained frequency-triad region. $B_{\max}$ was determined separately for each record.
Displayed frequency triads	$\lvert f_1 \rvert \leq 4.5$ kHz, $\lvert f_2 \rvert \leq 4.5$ kHz, and $\lvert f_1 + f_2 \rvert \leq 4.5$ kHz.

For context, Part I also examined an intact region of the same specimen using the same experimental procedure [3]. The intact response exhibited a different spectral pattern, with a dominant component near 5 kHz, whereas the response measured above the artificial delamination was dominated by a local component near 1 kHz. Under the small-impact condition, an additional component near 2 kHz was observed at the delamination location. The present Part II analysis focuses specifically on the higher-order spectral structure of the responses measured at that known delamination location.

To illustrate the difference between conventional and higher-order spectral representations, Figure 2 compares the normalized power spectrum and the bispectrum magnitude obtained from the same small-impact response.

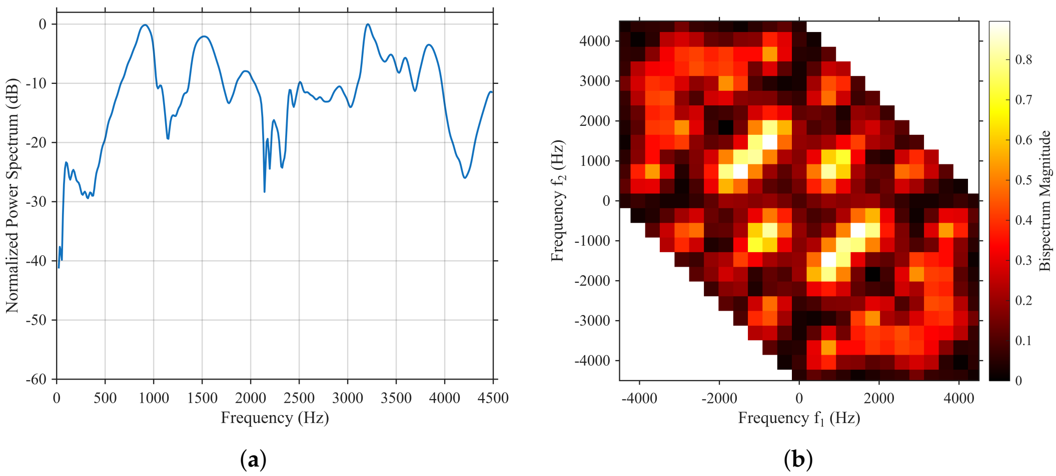

Figure 2. Comparison of conventional and higher-order spectral representations for the same small-impact response: (**a**) normalized power spectrum showing the distribution of signal power with frequency; (**b**) bispectrum magnitude showing third-order statistical relationships among frequency components associated with the triplet $(f_1, f_2, f_1 + f_2)$.

Figure 2a provides a one-dimensional representation of the spectral content and identifies the frequencies at which the measured response contains appreciable power. However, the power spectrum does not indicate whether different frequency components participate in third-order statistical relationships. Figure 2b introduces a second frequency axis and shows how pairs of frequencies f_1 and f_2 are associated with the sum frequency $f_1 + f_2$. The distributed local features in the bispectrum therefore provide information about higher-order spectral structure that is not available from the conventional power spectrum alone. The numerical scales of the two panels are not directly comparable because the power spectrum is normalized and expressed in decibels, whereas the bispectrum panel shows bispectrum magnitude.

3.2. Response Under Very Small Impact

Figure 3 presents the normalized vibration response, third-order cumulant, bispectrum magnitude, and bispectrum phase for the very-small-impact case.

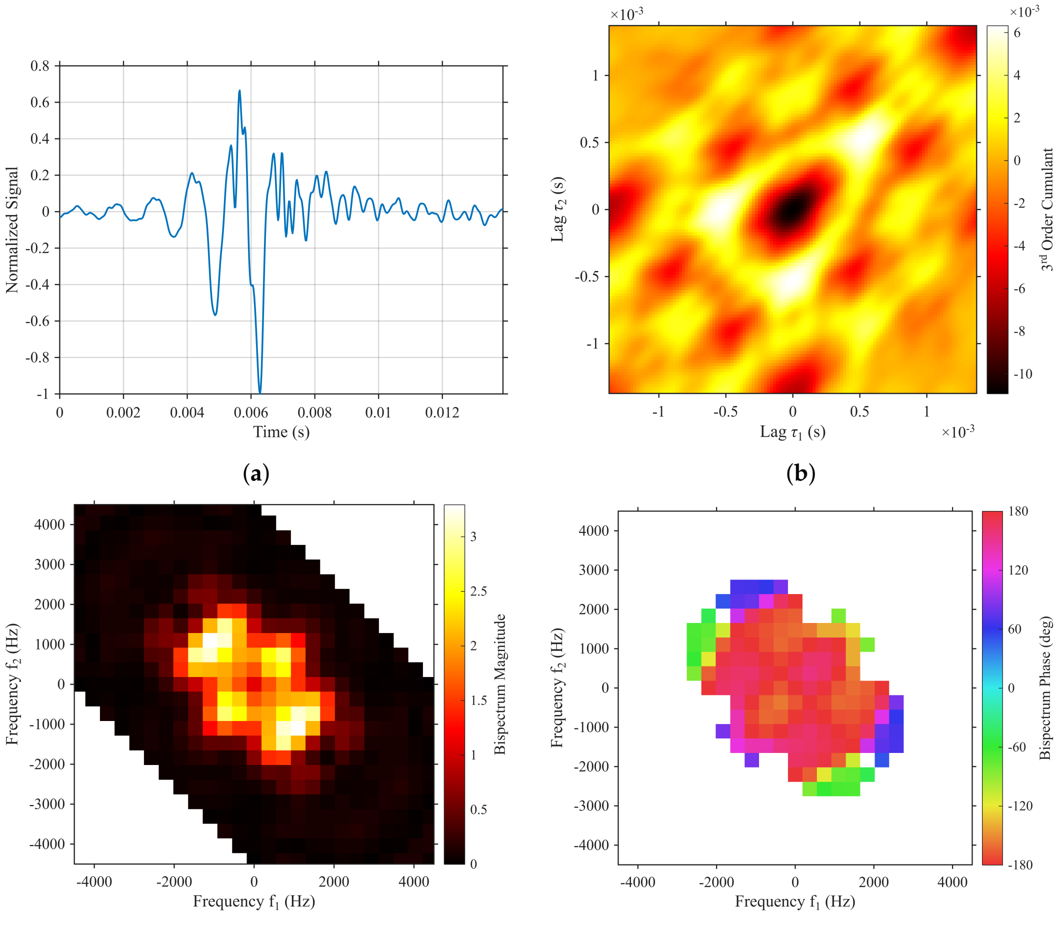

Figure 3. Measured response and higher-order spectral quantities at the delamination location under very small impact excitation: (**a**) normalized vibration waveform; (**b**) third-order cumulant; (**c**) bispectrum magnitude; and (**d**) bispectrum phase. Bispectral results are restricted to the frequency triads defined by Equation (36). In panel (**d**), phase is displayed only where the corresponding bispectrum magnitude is at least 5% of $B_{\max}$ for the record.

Figure 3a shows a short transient response. The largest oscillations occur approximately between 4 and 8 ms. A decaying ring-down follows the main response, and the signal approaches a relatively low amplitude near the end of the record.

The third-order cumulant in Figure 3b contains a pronounced localized structure near zero lag. A dominant negative region is surrounded by alternating positive and negative bands. The diagonal distribution of these features shows that the third-order dependence extends over several combinations of τ_1 and τ_2.

The corresponding bispectrum magnitude is shown in Figure 3c. Within the frequency region retained for physical interpretation, the dominant components are concentrated near the central portion of the bifrequency plane. Several distinct local maxima are visible within this region, while the surrounding components have lower magnitudes. The overall bispectral distribution therefore remains relatively concentrated.

https://doi.org/10.3390/vibration9030057

A nonzero bispectrum indicates third-order statistical dependence among frequency components. Under suitable conditions, this dependence can be associated with quadratic phase coupling [12,13,16]. However, a nonzero estimated bispectrum alone does not establish structural nonlinearity. The measured impact response is transient and has finite duration, and these factors can affect the estimate.

Figure 3d shows the biphase within the retained frequency-triad region. To avoid displaying phase values associated with very weak bispectral components, the phase is shown only where the corresponding bispectrum magnitude is at least 5% of B_{max} for this record. The displayed phase is therefore concentrated mainly around the bifrequency region containing the dominant bispectral components in Figure 3c. A cyclic color scale is used because phase is periodic, with -180° and 180° representing the same phase direction.

The bispectrum magnitude is shown in more detail in Figure 4. The three-dimensional representation in Figure 4a shows a concentrated group of dominant peaks surrounded by lower-magnitude components. The contour representation in Figure 4b shows the same distribution. The dominant components occupy a relatively limited portion of the retained bifrequency region, with weaker components surrounding the main group. This pattern is used as the reference for comparison with the small-impact case.

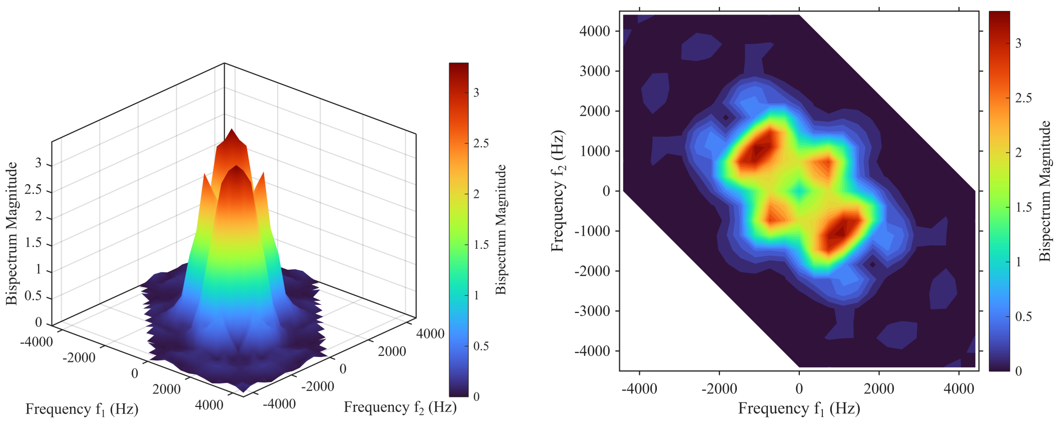

(**a**) (**b**)

Figure 4. Bispectrum magnitude of the response under very small impact excitation within the retained frequency-triad region: (**a**) three-dimensional surface representation; and (**b**) contour representation.

3.3. Response Under Small Impact

Figure 5 presents the corresponding results for the small-impact condition. The waveform in Figure 5a differs from the very-small-impact response. The main oscillatory event occurs approximately between 8 and 12 ms. It contains a denser sequence of oscillations and is followed by a longer ring-down that extends through much of the remaining record. Since the signals are normalized independently, the peak values in Figures 3a and 5a should not be used to compare their physical amplitudes.

The time–frequency behavior of these same responses was examined in Part I using spectrograms and wavelet scalograms [3]. That analysis showed greater spectral enrichment and more pronounced time-varying frequency content under the small-impact condition. The present bispectral analysis complements those results by examining third-order statistical dependence among the frequency components rather than their time-localized spectral amplitude alone.

The third-order cumulant in Figure 5b also differs from that of the very-small-impact response. Positive and negative regions are distributed over a larger portion of the lag plane. Several localized structures appear at different combinations of τ_1 and τ_2. The small-impact response therefore exhibits a more distributed third-order lag-domain structure.

The difference is also evident in the bispectrum magnitude shown in Figure 5c. Within the retained frequency region, the small-impact response exhibits a broader and more distributed bispectral pattern than the very-small-impact response. Multiple local maxima occur at different bifrequency combinations and extend farther from the center of the plane. The small-impact response therefore exhibits more prominent secondary features distributed over a broader portion of the bifrequency plane than the more concentrated pattern observed under the very small impact.

Figure 5d shows the corresponding biphase after application of the same 5% relative-magnitude display criterion. The displayed phase features extend over a broader set of bifrequency locations than in the very-small-impact case, consistent with the more distributed bispectrum magnitude in Figure 5c. Because the threshold is defined relative to the maximum magnitude of each record, this comparison describes the spatial distribution of the phase features and should not be interpreted as a quantitative comparison of phase-coupling strength.

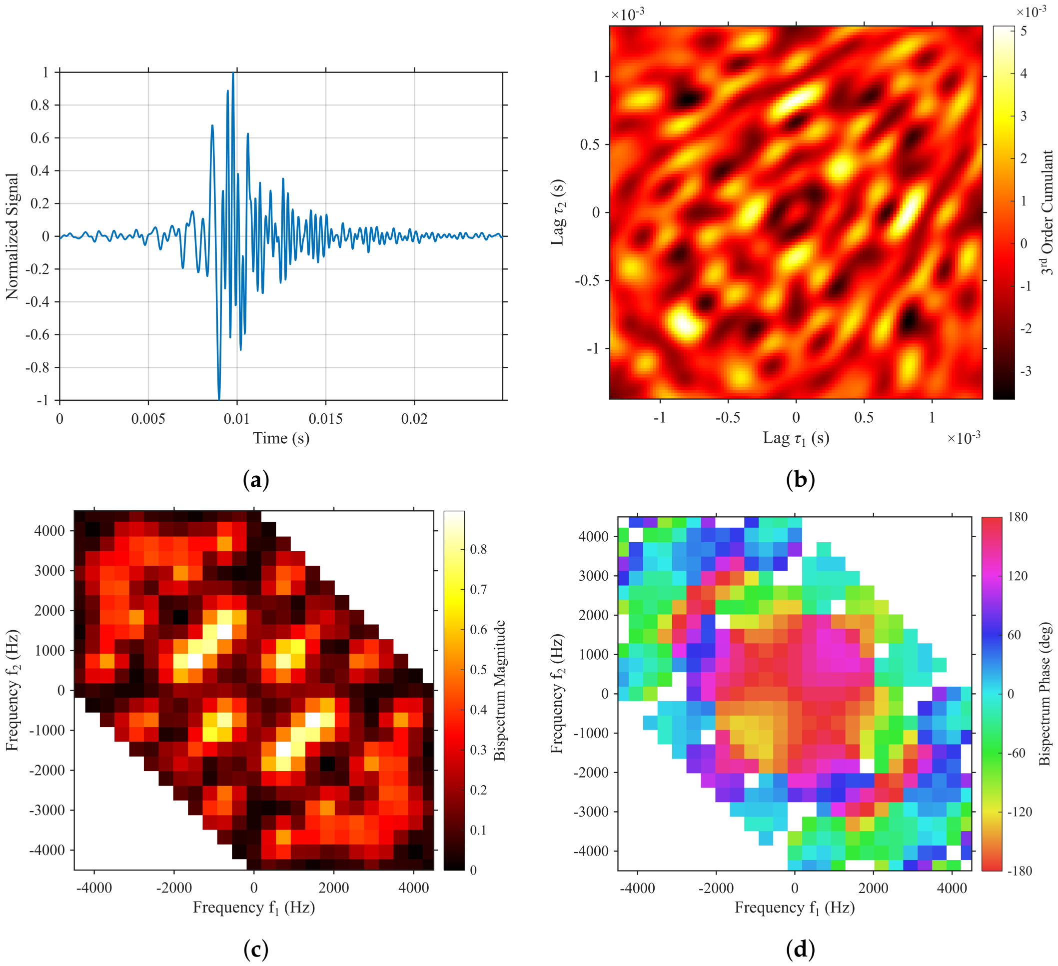

Figure 5. Measured response and higher-order spectral quantities at the delamination location under small impact excitation: (**a**) normalized vibration waveform; (**b**) third-order cumulant; (**c**) bispectrum magnitude; and (**d**) bispectrum phase. Bispectral results are restricted to the frequency triads defined by Equation (36). In panel (**d**), phase is displayed only where the corresponding bispectrum magnitude is at least 5% of $B_{\max}$ for the record.

3.4. Comparison of the Bispectral Characteristics

The bispectrum magnitude for the small-impact response is shown in surface and contour form in Figure 6.

Comparison of Figures 4 and 6 shows a clear difference within the frequency region retained for physical interpretation. The very-small-impact response contains a relatively concentrated group of dominant bispectral components. In contrast, the small-impact response exhibits a broader bispectral distribution with more prominent secondary features distributed over the bifrequency plane. The surface and contour representations show the same trend.

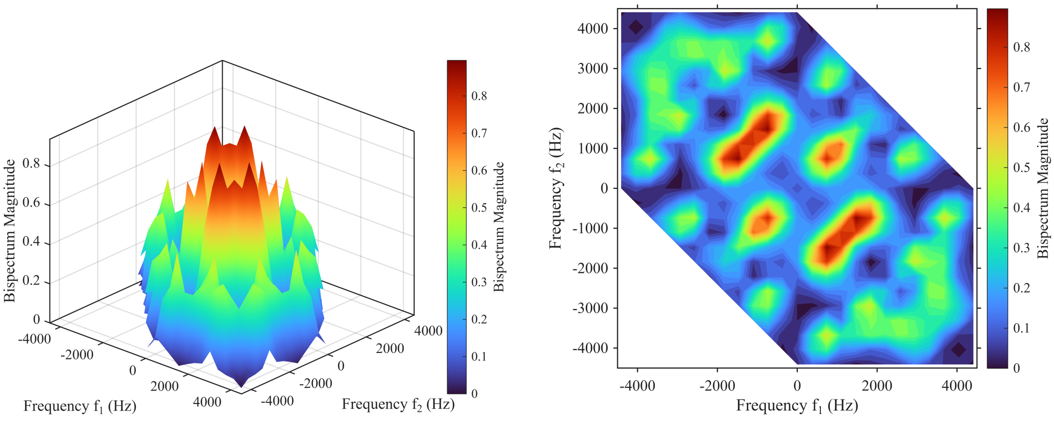

(**a**) (**b**)

Figure 6. Bispectrum magnitude of the response under small impact excitation within the retained frequency-triad region: (**a**) three-dimensional surface representation; and (**b**) contour representation.

To assess the influence of record duration, an equal-duration sensitivity analysis was performed using 614 samples for both responses, as shown in Figure 7.

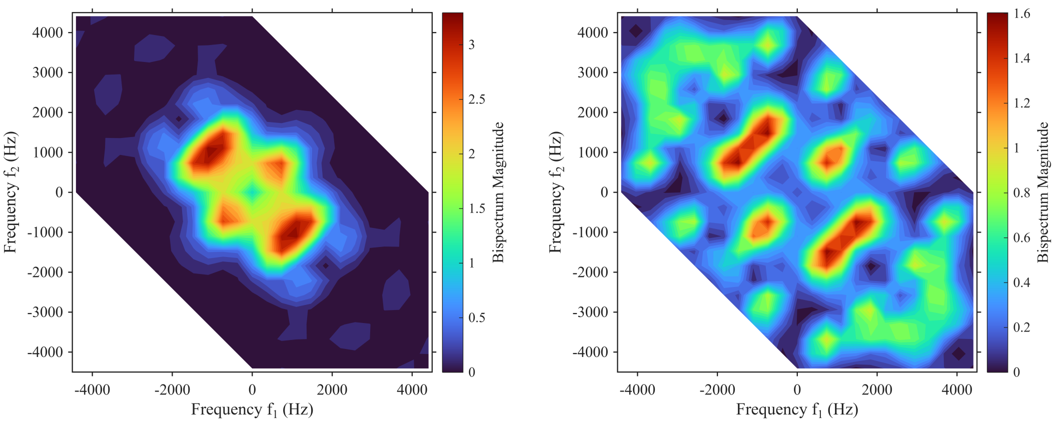

(**a**) (**b**)

Figure 7. Equal-duration sensitivity analysis of the bispectrum magnitude using 614 samples (13.923 ms) for both impact conditions: (**a**) very-small-impact response; (**b**) small-impact response. The same preprocessing and bispectral estimation parameters were used for both records. The small-impact response retains a broader and more distributed bispectral pattern after controlling for record duration.

The equal-duration sensitivity analysis confirmed that the main spatial difference between the two bispectral distributions was retained when both records were limited to 614 samples. The very-small-impact response remained relatively concentrated within the central bifrequency region, whereas the small-impact response retained a broader and more distributed pattern with multiple local features. A similar distinction remained in the third-order cumulant distributions. Truncation altered the numerical magnitudes and some fine local features of the finite-record estimates, but it did not remove the main qualitative difference in their spatial distributions. The conclusions are therefore based on the distribution and structure of the higher-order spectral components rather than on their absolute magnitudes.

The masked biphase distributions show a similar qualitative difference: phase features associated with appreciable bispectral magnitude are relatively concentrated for the very-small-impact response and more spatially distributed for the small-impact response. Because the 5% criterion is defined separately for each record, this observation is qualitative and does not represent a comparison of coupling strength.

These results are consistent with the measurements reported in Part I, where the small-impact condition introduced additional harmonic content [3]. The present analysis adds a third-order description of that change. The small-impact response exhibits a richer and more distributed bifrequency structure.

Representative nonzero-frequency triplets associated with prominent local bispectral maxima are listed in Table 2. Both impact conditions contain the same dominant triplet, $(f_1, f_2, f_1 + f_2) = (735, 735, 1470)$ Hz. For the small-impact response, the secondary triplet $(2572.5, 735, 3307.5)$ Hz has a relative magnitude of 0.588, corresponding to 58.8% of the dominant peak within that record. In contrast, the next strongest representative triplet for the very-small-impact response, $(2572.5, 1470, 4042.5)$ Hz, has a relative magnitude of only 0.040, or approximately 4.0% of its dominant peak. This difference supports the observation that the very-small-impact bispectrum is strongly concentrated around one dominant interaction, whereas the small-impact response contains a substantially more prominent secondary component. The reported relative magnitudes are normalized within each record and are used only to describe the distribution of the bispectral peaks, not to compare absolute nonlinear coupling strength between impact conditions.

Table 2. Representative nonzero-frequency bispectral triplets associated with prominent local maxima. Relative magnitude is normalized by the largest bispectral magnitude within each individual record.

Impact Condition	f_1 (Hz)	f_2 (Hz)	$f_1 + f_2$ (Hz)	Relative Magnitude
Very small	735.0	735.0	1470.0	1.000
Very small	2572.5	1470.0	4042.5	0.040
Small	735.0	735.0	1470.0	1.000
Small	2572.5	735.0	3307.5	0.588

The results should therefore be interpreted as evidence of a change in higher-order spectral structure between the two impact conditions, rather than as a quantitative measure of nonlinear coupling strength. The raw bispectrum is not a normalized coupling measure. A normalized quantity such as bicoherence would be more appropriate for this purpose [12,13]. However, reliable bicoherence estimation generally requires sufficient ensemble or segment averaging, which is difficult to obtain from the short transient records considered here without substantially reducing frequency resolution. Quantitative bicoherence analysis is therefore reserved for future experiments specifically designed to provide sufficient repeated or segmented data.

The experimental scope should also be recognized. The present Part II study examines higher-order spectral changes at a known artificial delamination location and should be regarded as a proof-of-concept characterization. The results do not establish universality across delamination sizes, depths, shapes, measurement positions, or structural materials. Validation over multiple defect configurations and spatial measurement locations is required before generalized diagnostic criteria can be established.

Although the nonlinear-oscillator and higher-order spectral framework is not mathematically restricted to concrete, the experimental validation presented here is specific to the tested concrete specimen. Application to composites, metallic plates, or other layered solids would require recalibration because defect-interface behavior, local modal frequencies, damping, sensor response, and wave propagation differ among materials and geometries. Field implementation would also need to account for environmental and operational noise, sensor coupling and placement, impact repeatability, boundary-condition variability, and the influence of finite record length on higher-order spectral estimation.

Overall, the experimental results show a consistent change in the higher-order response. The very-small-impact case is characterized by a relatively concentrated bispectral distribution. The small-impact case exhibits a broader, more distributed, multi-feature pattern within the calibrated interpretation region. The third-order cumulant shows a similar change from a localized lag-domain structure to a more distributed one. These observations complement the conventional spectral results reported in Part I and are consistent with the higher-order interactions represented by the Volterra-series formulation developed in Section 2.

4. Conclusions

This study extended the nonlinear delamination-characterization approach developed in Part I by introducing a Volterra-series formulation and higher-order spectral analysis. The local response of the delaminated region was represented using a nonlinear oscillator with quadratic and cubic stiffness terms. A third-order Volterra approximation was used to relate these nonlinear terms to the fundamental, second-harmonic, and third-harmonic components of the response.

The experimental impact responses reported in Part I were then examined using the third-order cumulant and bispectrum. Two excitation conditions were considered. Under the very small impact, the third-order cumulant showed a dominant localized structure, and the bispectral components were relatively concentrated within the retained bifrequency region. Under the small impact, the cumulant became more distributed over the lag plane. The bispectral pattern also became broader and more distributed, with more prominent secondary features.

Because the two records were normalized independently, their absolute bispectrum magnitudes were not compared quantitatively. An equal-duration sensitivity analysis using 614 samples for both conditions retained the main qualitative difference between the two bispectral distributions, indicating that the broader small-impact pattern is not solely a consequence of the different original record durations. The main difference between the two conditions is therefore the distribution and complexity of the higher-order spectral content. The small-impact response exhibits a broader and more distributed bispectral structure than the very-small-impact response. This change is consistent with the additional harmonic content reported in Part I and with a more distributed set of higher-order frequency interactions.

Bispectral analysis provides information that complements conventional FFT and power-spectrum analysis. The power spectrum describes the strength of individual frequency components, whereas the bispectrum provides information about third-order statistical dependence and phase relationships among frequency components. In the present measurements, these quantities reveal changes in the higher-order spectral structure that are not described by spectral amplitude alone.

The results should be interpreted as a comparative characterization of the two impact conditions. Accordingly, the observed change in higher-order spectral structure with impact condition should not be interpreted as equivalent to a validated criterion for identifying delamination in an unknown structure. The measured responses are transient and finite in duration, and a nonzero estimated bispectrum alone does not establish structural nonlinearity. In addition, the raw bispectrum is not a normalized measure of coupling strength. Future work will consider additional impact conditions and delamination configurations and will investigate normalized higher-order measures, such as bicoherence, for quantitative comparison of nonlinear frequency coupling. These developments may further support the use of higher-order spectral features for delamination detection and characterization in solid structures.

Author Contributions: Conceptualization, methodology, formal analysis, and visualization, G.S.C. and Y.S.; resources, I.W. and A.S.; data curation, G.S.C. and Y.S.; writing—original draft preparation, Y.S. and G.S.C.; writing—review and editing, Y.S., A.S., L.H. and G.S.C.; supervision, G.S.C. and Y.S.; funding acquisition, A.S.; All authors have read and agreed to the published version of the manuscript.

Funding: This research received internal support from the Battery Research Institute at Marshall University and received no external funding.

Data Availability Statement: The raw data supporting the conclusions of this article will be made available by the authors on request.

Acknowledgments: The authors gratefully acknowledge the Battery Research Institute-Marshall University for partially funding this research. The authors used an AI-based language tool to improve the grammar, clarity, and readability of the manuscript. The tool was not used to generate scientific content, analyses, results, or conclusions. The authors reviewed and edited the output and take full responsibility for the content of this publication.

Conflicts of Interest: The authors declare no conflicts of interest.

Abbreviations

The following abbreviations are used in this manuscript:

FFT	Fast Fourier Transform
HFRF	Higher-Order Frequency-Response Function

References

1. Kee, S.H.; Lee, J.W.; Candelaria, M.D. Evaluation of delamination in concrete by IE testing using multi-channel elastic wave data. *Sensors* **2020**, *20*, 201. [CrossRef] [PubMed]
2. Sun, D.; Sardahi, Y.; Chen, G.S.; Zatar, W.; Nghiem, H.; Yang, Z. A Study on Nonlinear Vibrations in the Impact-Echo Method for Void Flaw Detection in Solids. *Vibration* **2025**, *8*, 66. [CrossRef]
3. Sardahi, Y.; Salem, A.; Wait, I.W.; Chen, G.S.; McCormick, K.; Blake, K.; Samples, T.; Lanham, L. A Nonlinear Approach to the Delamination Characterization of Solid Structures Using Impact Response—Part I. *Vibration* **2026**, *9*, 15. [CrossRef]
4. Yuan, S.; Liu, P.; Chen, J.; Ren, Y.; Yang, Y.; Xu, Z.D. Laser Ultrasonic Detection for Strut Defects in Additively Manufactured Lattice Structure Using Zero-Group-Velocity Lamb Waves. *Ultrasonics* **2026**, *168*, 108223. [CrossRef] [PubMed]
5. Liu, P.; Yi, K.; Sohn, H.; Jeon, I.; Xu, Z.D. Grain Size Estimation in Additively Manufactured Metal Thin-Wall Using Noncontact Laser Ultrasonic and Zero-Group-Velocity Lamb Waves. *Mech. Syst. Signal Process.* **2026**, *242*, 113647. [CrossRef]
6. Chen, Z.H.; Entezami, A.; Sarmadi, H.; Xu, Z.D.; Gao, W.; Liu, L.; Behkamal, B. Transformer-Based Contrastive Denoising Autoencoder for Unsupervised Detection of Wind-Induced Vibration Changes in Cable-Supported Bridges. *Comput.-Aided Civ. Infrastruct. Eng.* **2026**, *49*, 100114. [CrossRef]
7. Hammami, M.; El Mahi, A.; Karra, C.; Haddar, M. Nonlinear Behaviour of Glass Fibre Reinforced Composites with Delamination. *Compos. Part B Eng.* **2016**, *92*, 350–359. [CrossRef]
8. Dolbachian, L.; Harizi, W.; Aboura, Z. Experimental linear and nonlinear vibration methods for the structural health monitoring (SHM) of polymer-matrix composites (PMCs): A literature review. *Vibration* **2024**, *7*, 281–325. [CrossRef]
9. Tewelde, S.A.; Krawczuk, M. Detection of Closing Cracks in Beams Based on Responses Induced by Harmonic Excitation. *Sensors* **2024**, *24*, 247. [CrossRef] [PubMed]
10. Kang, X.; Ma, S.; Wang, X.; Zhang, A.; Hu, J.; Xia, G. Nonlinear Dynamics of Low Frequency Compact Piezoelectric Energy Harvesting Vibration System by a Cucurbit Flute-Inspired Beam with Intelligent Adjustable. *Chaos Solitons Fractals* **2026**, *208*, 118315. [CrossRef]

11. Ma, S.; Kang, X.; Wang, X.; Hu, J.; Xia, G.; Zhang, W. Nonlinear Dynamics of Low Frequency Vibration Energy Harvesting Based on Flute-Shaped Slider Design. *Eur. J. Mech.—A/Solids* **2026**, *120*, 106221. [CrossRef]
12. Mendel, J.M. Tutorial on Higher-Order Statistics (Spectra) in Signal Processing and System Theory: Theoretical Results and Some Applications. *Proc. IEEE* **1991**, *79*, 278–305. [CrossRef]
13. Collis, W.B.; White, P.R.; Hammond, J.K. Higher-Order Spectra: The Bispectrum and Trispectrum. *Mech. Syst. Signal Process.* **1998**, *12*, 375–394. [CrossRef]
14. Rivola, A.; White, P.R. Bispectral Analysis of the Bilinear Oscillator with Application to the Detection of Fatigue Cracks. *J. Sound Vib.* **1998**, *216*, 889–910. [CrossRef]
15. Hillis, A.J.; Neild, S.A.; Drinkwater, B.W.; Wilcox, P.D. Global Crack Detection Using Bispectral Analysis. *Proc. R. Soc. A Math. Phys. Eng. Sci.* **2006**, *462*, 1515–1530. [CrossRef]
16. Nichols, J.M.; Marzocca, P.; Milanese, A. On the Use of the Auto-Bispectral Density for Detecting Quadratic Nonlinearity in Structural Systems. *J. Sound Vib.* **2008**, *312*, 726–735. [CrossRef]
17. Nichols, J.M.; Olson, C.C. Optimal Bispectral Detection of Weak, Quadratic Nonlinearities in Structural Systems. *J. Sound Vib.* **2010**, *329*, 1165–1176. [CrossRef]
18. Hickey, D.; Worden, K.; Platten, M.F.; Wright, J.R.; Cooper, J.E. Higher-Order Spectra for Identification of Nonlinear Modal Coupling. *Mech. Syst. Signal Process.* **2009**, *23*, 1037–1061. [CrossRef]
19. Cui, L.; Xu, H.; Ge, J.; Cao, M.; Xu, Y.; Xu, W.; Sumarac, D. Use of Bispectrum Analysis to Inspect the Non-Linear Dynamic Characteristics of Beam-Type Structures Containing a Breathing Crack. *Sensors* **2021**, *21*, 1177. [CrossRef] [PubMed]
20. Czeluśniak, K.; Staszewski, W.J.; Aymerich, F. Local Bispectral Characteristics of Nonlinear Vibro-Acoustic Modulations for Structural Damage Detection. *Mech. Syst. Signal Process.* **2022**, *178*, 109199. [CrossRef]
21. Yang, D.; Wang, K.; Zhang, J.; Yuan, Y.; Liu, Y.; Au, F.T.K. Micro-Crack Localization for Steel Strands Using Nonlinear Vibro-Acoustic Modulation Based on Modified Signal Bispectrum Analysis. *Measurement* **2024**, *233*, 114746. [CrossRef]
22. Zhang, J.; Wang, K.; Yang, D.; Yuan, Y.; Yang, S. Nonlinear Vibro-Acoustic Modulation for Microcrack Detection of Steel Strands Based on S-Transform Bispectrum. *Appl. Acoust.* **2025**, *227*, 110237. [CrossRef]
23. Schetzen, M. *The Volterra and Wiener Theories of Nonlinear Systems*; John Wiley & Sons: Hoboken, NJ, USA, 1980.
24. Nam, S.W.; Powers, E.J. Application of Higher Order Spectral Analysis to Cubically Nonlinear System Identification. *IEEE Trans. Signal Process.* **1994**, *42*, 1746–1765. [CrossRef]
25. Cheng, C.M.; Peng, Z.K.; Zhang, W.M.; Meng, G. Volterra-Series-Based Nonlinear System Modeling and Its Engineering Applications: A State-of-the-Art Review. *Mech. Syst. Signal Process.* **2017**, *87*, 340–364. [CrossRef]
26. Shiki, S.B.; da Silva, S.; Todd, M.D. On the Application of Discrete-Time Volterra Series for the Damage Detection Problem in Initially Nonlinear Systems. *Struct. Health Monit.* **2017**, *16*, 62–78. [CrossRef]
27. Villani, L.G.; Da Silva, S.; Cunha, A., Jr. Damage detection in uncertain nonlinear systems based on stochastic Volterra series. *Mech. Syst. Signal Process.* **2019**, *125*, 288–310. [CrossRef]
28. Fackrell, J.; White, P.; Hammond, J.; Pinnington, R.; Parsons, A. The Interpretation of the Bispectra of Vibration Signals—I. Theory. *Mech. Syst. Signal Process.* **1995**, *9*, 257–266. [CrossRef]
29. Hinich, M.J. Detecting a Transient Signal by Bispectral Analysis. *IEEE Trans. Acoust. Speech Signal Process.* **1990**, *38*, 1277–1283. [CrossRef]
30. PCB Piezotronics. Model 352B30 ICP® Accelerometer—Specification Sheet. Available online: https://www.pcb.com/contentstore/docs/PCB_Corporate/Vibration/Products/Manuals/352B30.pdf (accessed on 11 February 2026).
31. PCB Piezotronics. Model 482A22 Sensor Signal Conditioner—Specification Sheet. Available online: https://www.pcb.com/contentstore/docs/PCB_Corporate/Electronics/products/specsheets/482A22_J.pdf (accessed on 11 February 2026).
32. McMurray, T. bisp3cum. MATLAB Central File Exchange. 2000. Available online: https://www.mathworks.com/matlabcentral/fileexchange/60-bisp3cum (accessed on 14 August 2026).